C. R. Palevol 9 (2010) 445–454

Contents lists available at ScienceDirect

Comptes Rendus Palevol

www.sciencedirect.com

General palaeontology

Virtual reconstruction of the Neandertal lower limbs with an estimation of hamstring muscle moment arms

Reconstruction virtuelle d'un modèle de membres inférieurs de Néandertalien avec une estimation des moments musculaires des muscles ischiojambiers

Tara Chapman[a,*], Fedor Moiseev[a], Victor Sholukha[a], Stéphane Louryan[a,b], Marcel Rooze[a], Patrick Semal[c], Serge Van Sint Jan[a]

[a] *Laboratory of Anatomy, Biomechanics and Organogenesis (LABO), Faculty of Medicine, Université Libre de Bruxelles (ULB), Lennik Street 808, 1070 Brussels, Belgium*
[b] *Department of Radiology, ULB Erasme hospital, 1070 Brussels, Belgium*
[c] *Laboratory of Anthropology and Prehistory, Royal Belgian Institute of Natural Sciences, Vautier street 29, 1000 Brussels, Belgium*

ARTICLE INFO

Article history:
Received 28 February 2010
Accepted after revision 30 July 2010
Available online 5 November 2010

Written on invitation of the Editorial Board

Keywords:
Neandertal
Biomechanics
Locomotion
Moment arm

ABSTRACT

A major problem of fossil hominid analysis is a lack of complete specimens. Many individual specimens have been damaged by the effects of diagenesis and excavation. Significant advances in the field of three dimensional image processing (3D) have enabled the creation of accurately scaled reconstructions of individual fossil bones using mirrored parts of the same fossil bone or human/fossil hominid equivalents. This study presents, for the first time, a method to reconstruct a 3D virtual model of the lower limb of the Neandertal using different bones from different fossil remains (Spy II, Neandertal 1 and Kebara 2) and integrating them into a single model of the Neandertal lower limb. A biomechanical analysis of the model was performed, including computer graphics visualization of the results, motion displacement graphs and muscle moment arms. The overall method has been implemented into an open-source customized software (lhpFusionBox) developed for the biomechanical study of the musculoskeletal system.

Mots clés :
Néandertalien
Biomécanique
Locomotion
Moment musculaire

RÉSUMÉ

L'étude des fossiles d'hominidés se heurte souvent au problème de la découverte de spécimens incomplets, voire de fossiles endommagés par la diagenèse et/ou par les conditions de collecte. Les progrès récents dans le domaine de la morphométrie géométrique ont permis la remise à l'échelle et la reconstruction par symétrie de fossiles partiels ou manquants. Cet article présente une méthode originale permettant la reconstruction virtuelle tridimensionnelle d'un membre inférieur néandertalien. Celle-ci utilise, pour la reconstruction, des fossiles de différentes origines (Spy II, Neandertal 1 et Kebara 2) et les intègre dans un modèle validé. Une analyse biomécanique du modèle est ensuite réalisée (visualisation par infographie des modèles reconstruits, création des graphes de mouvements, analyse de mouvements musculaires, etc.). Un exemple d'analyse est présenté sur les muscles ischiojambiers. L'ensemble de la méthode a été intégré dans un logiciel développé dans le cadre d'une étude biomécanique relative à l'appareil musculosquelettique.

* Corresponding author.
E-mail address: tchapman@ulb.ac.be (T. Chapman).

1631-0683/$ – see front matter
doi:10.1016/j.crpv.2010.07.011

1. Introduction

Biomechanical analysis is useful in order to elucidate whether the distinct morphology of fossil hominids would have enabled a similar bipedal gait to anatomically modern humans. Analysis of locomotion in fossil hominids is difficult as motion data of fossil hominids is not available. Inferences about locomotion in fossil hominids has long been made by analysis of the external morphological surface, cortical bone distribution, limb proportions and body mass (e.g. Ruff, 2009; Steudel-Numbers and Tilkens, 2004; Trinkaus, 1981, 1983; Trinkaus et al., 1998). The use of computing technologies is now becoming increasingly popular in paleoanthropological reconstructions of fossil locomotion, employing techniques where models are created using anatomical data from living creatures (motion data) and fossils (digitization of bones) (Nicolas et al., 2007, 2009). These models include a bipedal robotic simulator, aiming to reproduce Lucy's locomotion with no proper input motion data (Sellers et al., 2004) and the combination of fossil hominid data with motion data on primates (Polk, 2004) and anatomically modern humans (Miller and Gross, 1998; Polk, 2004; Steudel-Numbers and Tilkens, 2004). However, a major problem of fossil hominid analysis in all studies is the lack of complete specimens in the fossil record, with many individual fossil specimens damaged by the impact of diagenesis and excavation. No single individual in the Neandertal fossil record preserves all the skeletal elements of the lower limb. Incomplete fossil hominids are therefore major obstacles to the analysis of locomotion and a scaled model of the lower limb skeleton is required for accurate analysis.

Reconstruction of fossil specimens to enable comparative analysis is a long-standing practice in paleoanthropology. Traditional reconstruction utilizes modeling materials to reconstruct missing parts and is often performed with a degree of artistic license (Kalvin et al., 1995; Leakey et al., 1991). Researchers are increasingly utilizing morphometrics and computer software to assist with reconstruction of fossil hominid material. Three-dimensional (3D) models are created from computed tomography (CT) scans or surface scans. Missing limbs or parts of damaged specimens are reconstructed by the use of anatomical landmarks, mirror imaging and the use of the limb counterpart or similar bone material from a similar or the same specimen (e.g. Benazzi et al., 2009; Kalvin et al., 1995; Neubauer et al., 2004; Ponce de León and Zollikofer, 1999). Missing parts have been completed utilising various geometrical techniques, for example, thin-plate spline warping (e.g. Benazzi et al., 2009; Neubauer et al., 2004) and multiple regression expectation-maximization algorithms (e.g. Gunz et al., 2004, 2009; Weaver and Hublin, 2009).

Virtual reconstruction in fossil hominids has tended to focus on the crania (e.g. Gunz et al., 2004, 2009; Kalvin et al., 1995; Neubauer et al., 2004; Ponce de León and Zollikofer, 1999) although recently, there are a growing number of studies virtually reconstructing postcrania, Ponce de León et al. (2008) on Neandertal infant and neonate skeletons, Weaver and Hublin (2009) and Berge and Goularas (2010) on the pelvis and Benazzi et al. (2009) on the clavicle. To date, however, none of these methods have created a composite lower limb model with different types of bones originating from different specimens. A fully articulated Neandertal skeleton has previously been reconstructed using traditional methods for museum purposes (Sawyer and Maley, 2005), although there has not been a scaled reconstruction, which is validated.

The Neandertals are extinct and therefore, there is no biological material to analyse muscles. Some biomechanical parameters (such as muscle excursion or muscle moment arms) are consequently impossible to measure directly. A moment arm indicates the distance between the main line of action of a particular muscle and the center of a joint crossed and moved by this muscle. A larger moment arm will allow a higher mechanical advantage than a reduced one. Muscles with larger moment arms can show a smaller fibre volume than muscles with smaller moment arms to perform the same amount of work (Brand and Hollister, 1992; Lieber, 2002).

Studies on the comparative locomotive analysis via skeletal analysis and limb length of the Neandertal skeleton and anatomically modern humans have conferred both locomotor advantages and disadvantages for Neandertals (e.g. Gruss, 2007; Kramer and Eck, 2000; Polk, 2004; Steudel-Numbers and Tilkens 2004). Rak and Arensburg (1987) have suggested that the morphological differences in the Neandertal pelvis may be attributable to locomotion and posture-related mechanics, although other researchers on the Neandertal lower limb have stated that Neandertals were likely to have had a similar bipedal gait to anatomically modern humans (Trinkaus, 1983, 1985; Trinkaus and Ruff, 1989). Previous studies, which assume a modern human-like locomotion in Neandertals, have documented a higher mechanical advantage, greater bending moments and larger moment arms in Neandertals as opposed to anatomically modern humans (e.g. Ruff, 1995, 2009; Trinkaus, 1983; Trinkaus and Ruff, 1989). Following the suggestion by Ruff (1995) that robusticity of the Neandertal pelvis and femur produced a significantly greater mechanical advantage compared to the human specimen, we aimed to test this hypothesis and to perform a quantified comparative analysis between skeletal motion, robustness and muscle moment arms.

Simulation systems exist to analyse the musculoskeletal behaviour of the human body, including moment arm length (e.g. Delp et al., 1990). Following the proposal from Trinkaus (1983) that Neandertals may have had 'sustained levels of activity over irregular terrain and this would have increased the knee extensor and ankle plantar flexor moment generating capacities in Neandertals' (Trinkaus, 1983, p. 458), Miller and Gross (1998) examined knee extensor moment arms in Neandertals using the SIMM musculoskeletal system developed by Delp et al. (1990). The software for these systems allows the simulation and analysis of various biomechanical parameters related to muscle physiology during given motions. Miller and Gross's (1998) Neandertal model did not give details of the scaling method and was created by modifying muscle insertion sites on a model of a modern human, and not on Neandertal remains.

The first aim of this study was therefore to develop a novel and validated method to fuse different skeletal elements together (i.e., a particular bone, in our case the pelvis, to a differing bone, e.g. the femur, obtained from another specimen). The second aim was to reconstruct a single integrated Neandertal lower limb model by applying the developed method in the first aim. The third aim of this study was to use the integrated Neandertal lower limb model developed in the second aim to perform an analysis of the knee flexor moment arms (i.e., hamstring muscles). Note that the third aim is part of a running project and only preliminary results are presented in this paper.

2. Materials and methods

As no single Neandertal specimen preserves all the skeletal elements of the lower limb, we used the Kebara 2 pelvis as it is the most complete Neandertal pelvis found to date. The Kebara 2 pelvis has been the subject of considerable debate. See Andersen (1989) for a review of early hypotheses. The morphology of the Kebara 2 pelvis does not significantly differ in size from modern humans but there are important morphological differences. Similar to other Neandertal specimens, there is an unusually wide sub-pubic angle (110°), a different orientation of the acetabulae and an extended pubis symphysis (Rak, 1991; Rak and Arensburg, 1987). The Neandertal 1 and Spy II skeletal remains both exhibit a fairly robust postcranial skeleton with large diaphyseal diameters of the femur relative to length, bowing and rounded shafts of the femora (Hrdlička, 1930; Trinkaus and Ruff, 1989).

The Kebara 2 pelvis was found in Israel and has been referenced as male, with an estimated age of 50–55,000 years old (Bar-Yosef et al., 1992). The Spy II specimen was found in Belgium, and has recently been dated as being approximately 36,000 years old (Semal et al., 2009). The

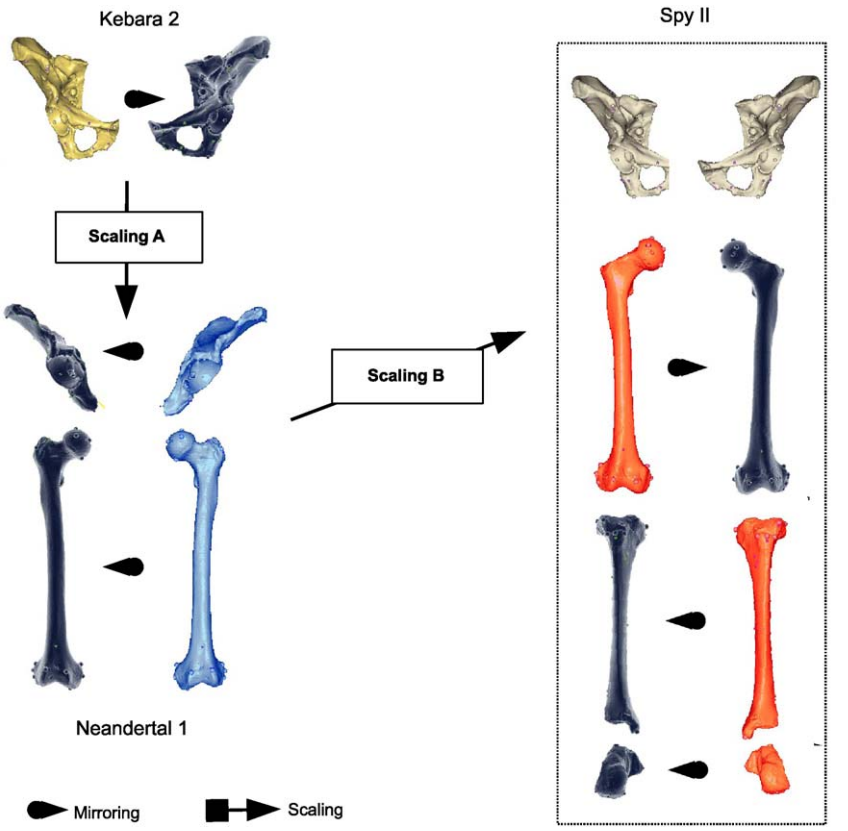

Fig. 1. Overall method for registration of Kebara 2 iliac (top left) to Spy II femur (right) using the Neandertal 1 iliac and femur (bottom left). This figure illustrates the two-stage scaling used in this paper (technical details about the procedure can be found in Table 2). The two-stage scaling was justified because a direct scaling of the Kebara 2 pelvis to Spy II dimensions was not possible as there are no common reference bones. The first stage (Scaling A) registers the Kebara 2 iliac to the Neandertal 1 iliac. The second stage (Scaling B) used the spatial transformation required to scale the Neandertal 1 femur to Spy II, to register the Kebara 2 pelvis to Spy II dimensions. Rounded arrows indicate mirroring, while plain arrows indicate scaling.

Fig. 1. Recalage de l'os iliaque de Kebara 2 (en haut et à gauche) vers les dimensions du fémur de Spy II (à droite), par utilisation de l'os iliaque et du fémur de Neandertal 1 (en bas et à gauche). Cette image illustre les deux étapes de la remise à l'échelle développée au cours de cette étude (les détails techniques de la méthode sont présentés dans le Tableau 2). Le recalage direct du pelvis de Kebara 2 vers Spy II n'est pas possible. La première étape (Scaling A) recale l'os iliaque de Kebara 2 vers le même os de Neandertal 1. La seconde étape (Scaling B) utilise la transformation spatiale nécessaire à recaler le fémur de Neandertal 1 vers celui de Spy II, pour recaler l'os iliaque de Kebara 2 (déjà transformé une première fois à la première étape) vers les dimensions de Spy II. Les flèches arrondies indiquent les opérations de « mirroring » ; les flèches normales indiquent les opérations de recalage.

Table 1
Specimens utilized in study.
Tableau 1
Spécimens utilisés dans cette étude.

Specimen	Material	State of preservation
Spy II skeleton		
Right femur	Original bones	Greater trochanter missing
Left tibia		Complete
Neandertal 1		
Left iliac bone (partial)	Casts of originals obtained with kind permission from the Neanderthal museum	Most of the pubic bone on the pelvis is missing, including superior and inferior ramus. The posterior inferior iliac spine is missing
Left femur		Complete with slight damage to distal lateral condyle
Kebara 2		
Right iliac bone	Cast of original obtained with kind permission from Yoel Rak	The medial end of pubis symphysis is missing

Neandertal 1 skeleton, found in Germany, has recently been dated as being approximately 40,000 years old (Schmitz et al., 2002).

The Spy II femur and tibia were used as they are relatively complete and the Neandertal 1 remains of pelvis and femur were used as an intermediate scaling stage as there are no common skeletal elements between Kebara 2 and Spy II (Fig. 1).

Spy II material and casts of bones were obtained from the Royal Belgian Institute of Natural Sciences and included (Table 1): Spy II skeleton (right femur (Spy 8), left tibia (Spy 9)), Neandertal 1 skeleton casts (left iliac bone, left femur) and Kebara 2 skeleton cast (right iliac).

All available bones and casts were processed by Computerized Tomography (CT) at the Laboratory of Anatomy, Biomechanics and Organogenesis (LABO), Université Libre de Bruxelles (ULB), Belgium (Siemens Volume Zoom) or at the Radiology Department of the ULB Erasme Hospital, (Siemens Sensation 64). Image settings were: image format = DICOM 3.0; image matrix = 512 × 512; slice thickness = between 0.3 mm and 1 mm. The DICOM image stacks were then imported into AMIRA, and segmented using automatic thresholding to create 3D geometrical models, which were stored in STL format. 3D images were then imported into a customized software, called lhpFusionBox, used in this study for all operations described below. This is an open-source software program, currently being designed for biomechanical and clinical studies, related to the musculoskeletal system of modern humans (Van Sint Jan et al., 2006; Viceconti et al., 2007a). The software allows almost any type of biomedical data to be imported, including medical images in DICOM format, gait analysis data and finite element analysis results (Viceconti et al., 2007b). It has recently been adapted for paleoanthropological analysis at ULB.

The available specimens were from different individuals and some specimens were partial remains. The Spy II remains did not include a pelvis. Kebara II has a well-preserved pelvis, but could not be directly scaled to Spy II since both specimens have no common bones. Spatial

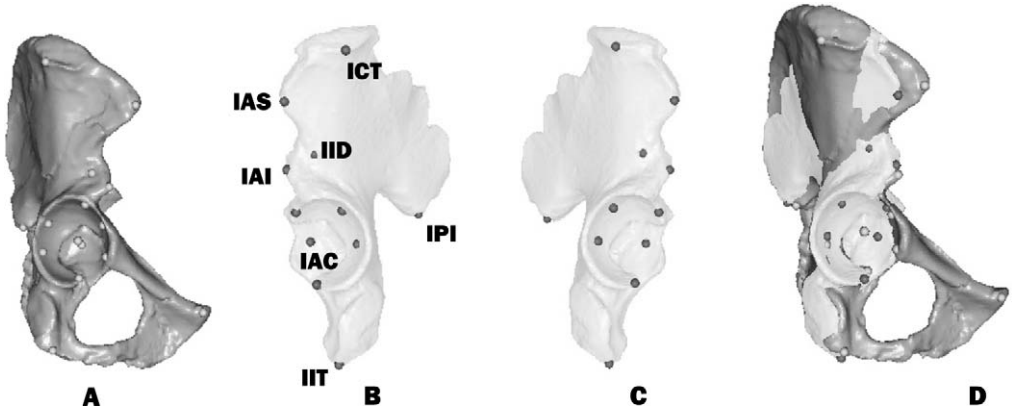

Fig. 2. Result of Scaling A. In dark grey = Kebara 2 (A, D), in light grey = Neandertal 1 (B, C, D). A: right iliac bone of Kebara 2. B: left iliac bone of Neandertal 1. C: mirrored B (result of step 4, see Table 3). D: registered Kebara 2 iliac or $RK2_{RN1^{mirror}}$ (result of step 5, see Table 3). Note the satisfactory match of the acetabular cavities between both 3D models on image D. RMS error was 10.8 mm.
Fig. 2. Résultats du recalage « Scaling A ». En gris clair = Kebara 2 (A, D), en gris foncé = Neandertal 1 (B, C, D). A : os iliaque droit de Kebara 2. B : os iliaque gauche de Neandertal 1. C : miroir de B (résultat de l'étape 4, voir Tableau 3). D : os iliaque de Kebara 2 après recalage ou $RK2_{RN1^{mirror}}$ (résultat de l'étape 5, voir Tableau 3). La congruence articulaire au niveau de l'acetabulum semble satisfaisante après recalage. L'erreur RMS relative à la position de l'ensemble des marqueurs utilisés fut de 10,8 mm.

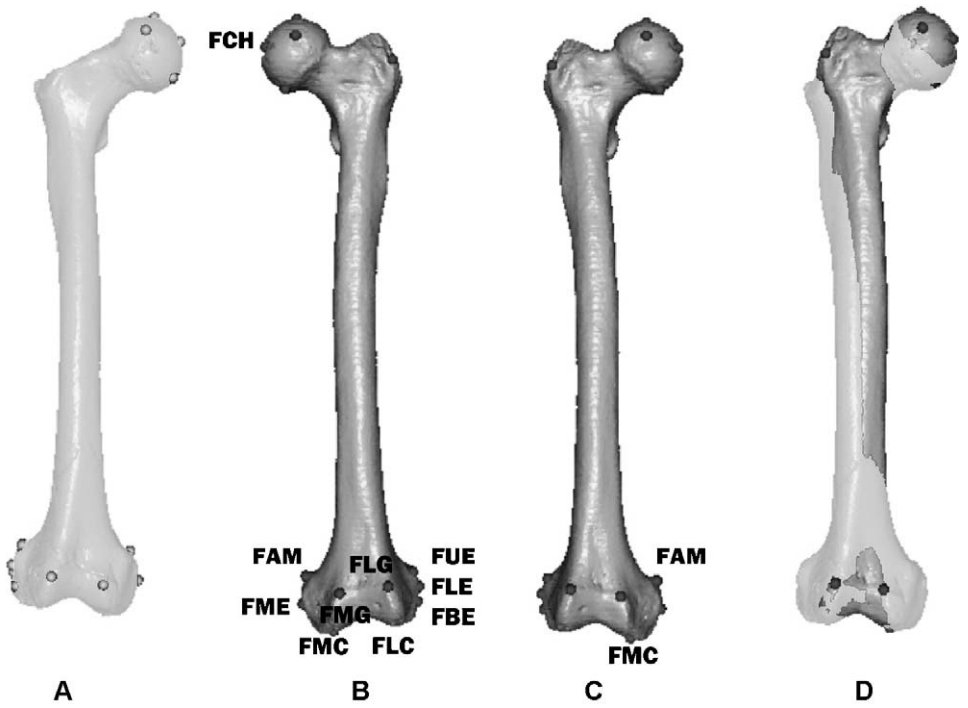

Fig. 3. Results of scaling of femurs (Scaling B, Steps 11 and 12). In light grey = Spy II (A, D), in dark grey = Neandertal 1 (B, C, D). A: *RS*2 femur (coloured in light grey). B: *LN*1 femur. C: $RN1^{mirror}$ femur (step 8). D: $RK2_{RN1^{mirror} \rightarrow RS2}$ femur obtained in step 14 using the transformation matrix $A_{RN1^{mirror} \rightarrow RS2}$ (determined in step 12). RMS error was 6.0 mm.

Fig. 3. Résultats du recalage des os fémoraux (Scaling 2, étapes 11 et 12). En gris clair = Spy II (A, D), en gris foncé = Neandertal 1 (B, C, D). A : fémur *RS*2 (coloré en gris clair). B : fémur *LN*1. C : fémur $RN1^{mirror}$ (étape 8). D : fémur $RK2_{RN1^{mirror} \rightarrow RS2}$ obtenu à l'étape 14 par utilisation de la matrice de transformation $A_{RN1^{mirror} \rightarrow RS2}$ (déterminée à l'étape 12). L'erreur RMS de la transformation fut de 6,0 mm.

locations of anatomical landmarks (ALs) were virtually palpated before performing data fusion of the various available fossils.

ALs are recognizable features on the surface of bones or 3D bone models. ALs were virtually palpated on all available 3D models (Figs. 2 and 3) using strictly defined and reproducible standardized AL definition from Van Sint Jan (2007). The following ALs were virtually palpated on the Kebara 2 Neandertal 1 pelves: anterior superior iliac spine (IAS), posterior inferior iliac spine (IPI), ischial tuberosity (IIT), crest tubercle (ICT) and center of acetabulum (IAC 3-7) (Fig. 2). The tubercle of the Adductor Magnus muscle (FAM), medial epicondyle (FME), medial sulcus (FMS, not visible on image), center (FLE), upper (FUE) and lower (FBE) aspect of lateral epicondyle crest, popliteal sulcus (FPS, not visible on image), anteriormedial (FMG) and anteriolateral (FLG) surface of the patellar surface groove, most distal point of the medial condyle (FMC) and lateral condyle (FLC) and center of the head (FCH 1-6) were palpated on the Neandertal 1 and Spy II femora (Fig. 3). The lateral (TTL), medial (TTM) and central (TTC) aspect of tibial tuberosity, medial (TMR) and lateral (TLR) ridge of tibial plateau, Gerdy's tubercle (TGT) and the apex of the medial malleolus (TAM) were palpated on the Spy II tibia.

Due to missing fossil fragments (Table 1), several standardized landmarks (Van Sint Jan, 2007) could not be palpated (the greater trochanter on Spy II femur, the most distal point of the lateral condyle on Neandertal 1 femur, two points of the acetabulum, posterior superior iliac spine and pubic spine on the Neandertal 1 iliac bone). To further strengthen the link during registration between the two iliac bones we created additional landmarks, which were clearly identifiable and palpable in both specimens (Fig. 2). These supplementary landmarks included the midsection of the internal sacroiliac joint (ISI, not visible on image), the anterior inferior iliac spine (IAI) and a small depression visible to the left on the lateral side of the anterior inferior iliac spine (IID), visible in both the Neandertal 1 and Kebara 2 iliac bones.

All 3D models were mirrored to create a full lower limb. The lhpFusionBox has been adapted to allow mirroring techniques to duplicate heterolateral counterparts of all available models with previously located ALs. This ensured that located ALs were exactly mirrored on their counterpart bones.

2.1. Fusion method for Scaling Kebara 2 to Spy II dimensions by two-stage registration

All three Neandertal specimens (Spy II, Neandertal 1 and Kebara 2) exhibit slightly different morphologies. The Spy lower skeleton (femur and tibia) and the Kebara 2 pelvis have no common skeletal elements that would enable straightforward scaling. Scaling methods found in literature process objects (i.e., bones) of the same nature: for example, a femur is scaled to another femur (Van Sint

Table 2
Logic of the double registration procedure allowing scaling of the Kebara 2 iliac bones to the more robust Spy II morphology. See text below for further details.
Tableau 2
Logique de la double procédure de recalage permettant la remise à l'échelle de l'os iliaque de Kebara 2, de constitution gracile, vers la morphologie plus robuste de Spy II. Voir texte pour plus de détails.

Stage 1 (from Kebara 2 to Neandertal 1):
1. Right Kebara 2, or *RK*2, iliac: virtual palpation of AL's (see above procedure description)
2. Mirroring of *RK*2 iliac and associated AL's to obtain Left Kebara 2 iliac or $LK2^{mirror}$ iliac
3. Left Neandertal 1 (*LN*1) iliac: virtual palpation of AL's
4. Mirroring of *LN*1 iliac (and AL's) to obtain Right Neandertal 1 iliac or $RN1^{mirror}$ iliac
5. Scaling of *RK*2 iliac to $RN1^{mirror}$ iliac. The result is an *RK*2 iliac scaled to the $RN1^{mirror}$ proportions. The new model is therefore called $RK2_{RN1^{mirror}}$
6. Scaling of $LK2^{mirror}$ iliac to *LN*1 iliac. The result is $LK2^{mirror}_{LN1}$ iliac

Stage 2 (from Neandertal 1 to Spy II):
7. *LN*1 femur: AL virtual palpation
8. Mirroring of *LN*1 (+ AL's) femur to obtain $RN1^{mirror}$ femur
9. Right Spy II (*RS*2) femur: AL virtual palpation
10. Mirroring of *RS*2 femur to obtain Left Spy II femur or $LS2^{mirror}$ femur
11. Determination of transformation matrix $A_{LN1\rightarrow LS2^{mirror}}$ between *LN*1 femur and $LS2^{mirror}$ femur
12. Determination of transformation matrix $RN1^{mirror}$ between $RN1^{mirror}$ femur and *RS*2 femur
13. Scaling of $LK2^{mirror}_{LN1}$ iliac to $LS2^{mirror}$ femur: $LK2^{mirror}_{LN1\rightarrow LS2^{mirror}} = A_{LN1\rightarrow LS2^{mirror}} \cdot LK2^{mirror}_{LN1}$
14. Scaling of $RK2_{RN1^{mirror}}$ iliac to *RS*2 femur: $RK2_{RN1^{mirror}\rightarrow RS2} = A_{RN1^{mirror}\rightarrow RS2} \cdot RK2_{RN1^{mirror}}$

Jan et al., 2002). To the authors' knowledge, no previous method in the anthropological sciences has reported a scaling method to process objects of a different nature (i.e., for example, scaling a pelvis to the dimensions of a particular femur). The fusion method presented here aimed to achieve this. The Neandertal 1 femur was used as an intermediate scaling stage between the Kebara and the Spy II dimensions (Fig. 1, Scaling A). The method is based on the assumption that relative pelvis size compared to femur and tibia size is the same in different individuals.

Model scaling was performed in lhpFusionBox via two stages using spatial data registration from the previously located ALs. The first scaling stage (Fig. 1, Scaling A) scaled the Kebara 2 iliac bone to the Neandertal 1 iliac bone (Table 2, steps 1 to 6). The second stage (Fig. 1, Scaling B; Table 3, steps 7 to 14,) scaled the result of the first stage to the Spy II femoral dimensions via the Neandertal 1 femoral dimensions. The scaling procedure was based on standard singular value decomposition, or SVD, algorithms (Challis, 1995; Horn, 1987).

Stage 1 in Table 2 (steps 1 to 6) is similar to standard spatial registration performed in the biomechanics field, i.e., registering bone models of the same kinds together (e.g., iliac with iliac, femur with femur). Steps 1 to 4 dealt with virtual palpation and mirroring of the various models. Step 5 scaled the original Kebara 2 right iliac bone (*RK*2) to the dimensions of the mirrored Neandertal 1 iliac bone ($RN1^{mirror}$). The same procedure was adopted for the heterolateral side (step 6). At the end of this stage, the Kebara 2 iliac bones showed Neandertal 1 proportions. The fitting of the joint is important for motion representation and to enable further motion analysis, it is therefore important that the joint registration is accurately scaled.

The above-described method enabled us to obtain a full lower limb model of a Neandertal (see results). In order to allow further musculoskeletal analysis, the entire model has been further registered to joint kinematics and motion data of an anatomically modern human (further details available from Sholukha et al. (2006)). The registration of the Neandertal model to the animated human data gives a detailed description, including a six degrees-of-freedom mechanism at knee and ankle joint levels, of motion pattern (Chapman et al., in press; Sholukha et al., 2006). This information also includes the hip, knee and ankle instantaneous helical axis (Van Sint Jan et al., 2002). The motion selected for this study was a squatting motion as this covered a large range in all joints. A similar model of a modern human was available for comparison with the Neandertal model. To analyse whether the robusticity of the Neandertal pelvis and femur produced a significantly greater mechanical advantage than the human specimen (Ruff, 1995), the size of the Neandertal model and Modern Human model were scaled to the same size.

On the two models, muscle attachments were manually located on the bony features available from the bone surfaces. Origins and insertions of the hamstring muscles (i.e., semi-membranosus m., semi-tendinosus m., long and short head of biceps femoris m) were located on the 3D models and processed to estimate the muscles' line of actions. Hamstrings knee moment arms were then processed from the distance between the hamstring muscle line of actions

Table 3
Comparative table with mean, minimal and maximal moment arms of Neandertals and Modern humans (in mm).
Tableau 3
Tableau comparatif des moments musculaires de Néandertaliens et d'Hommes modernes (moyenne, minimum, maximum) (en mm).

	Semi-semimembranosus			Semi-tendinosus			Biceps–short head			Biceps–long head		
	Mean	Min	Max	Mean	Min	Max	Mean	Min	Max	Mean	Min	Max
Neanderthal	30	5	60	97	52	110	31	26	36	26	17	36
Modern	28	13	52	80	50	89	25	22	28	23	18	28

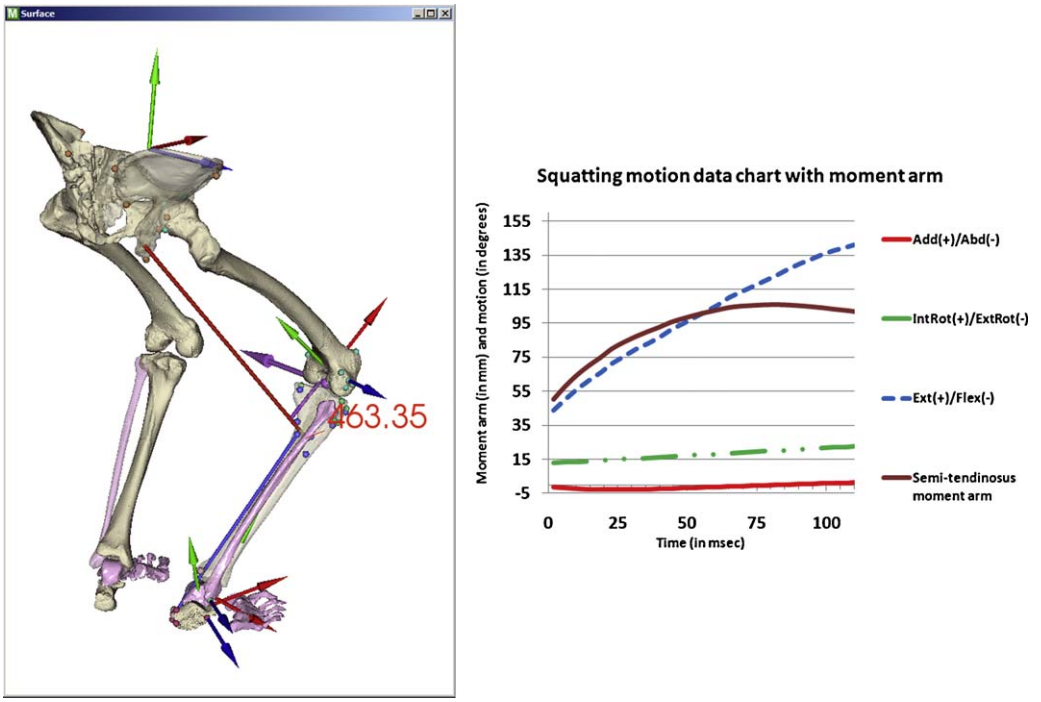

Fig. 4. Neandertal model obtained in this study and fused to a squatting motion of a modern human (screen snapshot from lhpFusionBox with graph). On the left: the model. The white bones are Neandertal fossil remains. The pink bones are the modern human bones. Anatomical reference frames were built on the hip, knee and ankle joint according to international recommendations (Wu et al., 2002). The knee motion axis is displayed (pink arrow). The line of action of the semi-tendinosus and moment arm are also visible. On the right: biomechanical graph from data obtained from the model. Motion representation is displayed (see caption in the figure; Add = adduction; Abd = abduction; Ext = extension; Flex = flexion; IntRot = internal rotation; ExtRot = external rotation). The semi-tendinosus m. moment arm is given by a full line. Similar results were obtained for the semi-membranosus m., the long head and short head of the biceps cruralis m. (not displayed here).

Fig. 4. Modèle virtuel de Néandertalien obtenu dans cette étude et fusionné à un mouvement effectué par un Homme moderne (capture d'écran à partir du programme lhpFusionBox avec graphe). À gauche : le modèle. Les os affichés en blanc sont obtenus à partir de fossiles néandertaliens. Les os affichés en rose sont des os d'Hommes modernes. Les référentiels techniques pour les articulations de la hanche, genou et cheville ont été construits selon des recommandations internationales (Wu et al., 2002). L'axe de mouvement du genou est aussi affiché (flèche rose). La ligne d'action du muscle semi-tendineux et son bras de levier instantané sont visibles. À droite : graphe biomécanique obtenu à partir du modèle. La représentation du mouvement est affichée (voir légende, Add = adduction ; Abd = abduction ; Ext = extension ; Flex = flexion ; IntRot = rotation interne ; ExtRot = rotation externe). Le moment musculaire du muscle semi-tendineux est donné par la courbe pleine. Un affichage similaire a été obtenu pour les muscles semi-membraneux et pour les têtes longue et courte du biceps crural (non illustré ici).

and the knee instantaneous helical axis (Fig. 4) (Brand and Hollister, 1992). Instantaneous helical axis, muscle line of action and muscle moment arms were directly processed within the LhpFusionBox interface.

3. Results

3.1. Reconstruction of Neandertal lower limb models

This section presents the results related to the first and second aims of this paper, which is the validated reconstruction of a model of the Neandertal lower limb.

Information on the dispersal of ALs between bones was given by the root mean square (RMS) error of the various ALs processed by a singular value decomposition (SVD) algorithm (Challis, 1995). The root mean square error is the square root of the average of the squared differences between landmarks. The dispersion of ALs between the Kebara 2 right iliac bone (*RK*2) and mirrored Neandertal 1 iliac bone ($RN1^{mirror}$) iliac bones led to a RMS error of 10.8 mm (Fig. 2).

Stage 2 in Table 2 (steps 7 to 14) further scaled the Kebara 2 iliac bone, scaled at this stage to Neandertal 1, to the Spy II morphology. The common reference point between Neandertal 1 and Spy II was the presence of an almost complete single femur in both skeletons. Scaling of the Kebara 2 iliac bone (scaled to Neandertal 1) to Spy II dimensions was performed using the femoral bones as intermediate scaling.

After virtual palpation and mirroring (steps 7 to 10), the transformation matrix $A_{LN1 \rightarrow LS2^{mirror}}$ allowed scaling from the Neandertal 1 femur (*LN*1) to the mirrored Spy II femur ($LS2^{mirror}$) (step 11). Results of this transformation led to a RMS error of 6.0 mm (Fig. 3). The same procedure was applied for the right. All bones were mirrored in the study and therefore RMS error was equal for both the left and right side.

The final step scaled Kebara 2 iliac bone model to Spy II dimensions using the available transformation matrices. The results of scaling stage 2 were the Kebara 2 iliac bones scaled to the Spy II morphology.

At this stage, the Kebara 2 pelvis was scaled to the dimensions of the Spy II remains and a pair of lower limbs, including the pelvis, femora and tibiae was available.

3.2. Hamstring moment arms of the knee

The Neandertal model integrated with the motion data of a human enabled visualisation, creation of anatomical axes, motion representation and the processing of specific biomechanical parameters with graphic output, e.g., related to muscle moment arms (Fig. 4).

Comparison of the muscle moment arms obtained from the Neandertal model and modern human model shows that the hamstring muscles seem to have a higher mechanical advantage in the Neandertal model (Fig. 5, Table 3). For example, the biceps femoris–short head muscle moment arm was on average 24% larger for Neandertals. The same trends were also found for the other hamstring muscle: semitendinosus = +21%, long biceps = +12%, and semimembranosus = +5%. These results seem to demonstrate that the available Neandertal specimen shows hamstring mechanical advantages compared to a modern human of the same size.

4. Discussion

4.1. Reconstructed Neandertal lower limb model

The scaling of Neandertal fossil material from different specimens is the first step to creating a scaled, full lower limb skeleton to enable accurate motion analysis. Standard spatial registration registers bone models of the same kinds together (e.g., pelvis with pelvis, clavicle with clavicle, cranium with cranium) (Benazzi et al., 2009; Gunz et al., 2004, 2009; Kalvin et al., 1995; Neubauer et al., 2004; Ponce de León and Zollikofer, 1999; Van Sint Jan et al., 2002; Weaver and Hublin, 2009). The new development in LhpFusionBox presented in this article enables the scaling of a particular bone using two iterations of different bones via spatial registration. The accuracy of the various geometrical transformations in which the models are processed were tracked via RMS errors.

Spatial data registration from the Neandertal 1 femur to the Spy II femur produced an RMS error of 6.0 mm. Kepple et al. (1998) found a mean RMS error of 6.6 mm from the comparison and registration of femora from 52 male and female anatomically modern human specimens. The results of Kepple et al. (1998) cannot be directly comparable to the RMS error demonstrated in the reconstructed Neandertal model as bony landmark palpation differed, although they do give an indication of the scale of RMS errors within a single species. The comparison of this mean value of RMS errors from the registration of femora between humans in the small study from Kepple et al. (1998), with the value of the registration between femora in Neandertals indicates that the morphology between the Neandertal 1 femur and the Spy II femur demonstrated an RMS error within the limits of registration of femora between humans. The comparatively small RMS error of 6.0 mm found between the Neandertal femora therefore gave us the justification of using the Neandertal 1 skeletal remains as a scaling reference for registration to Spy II.

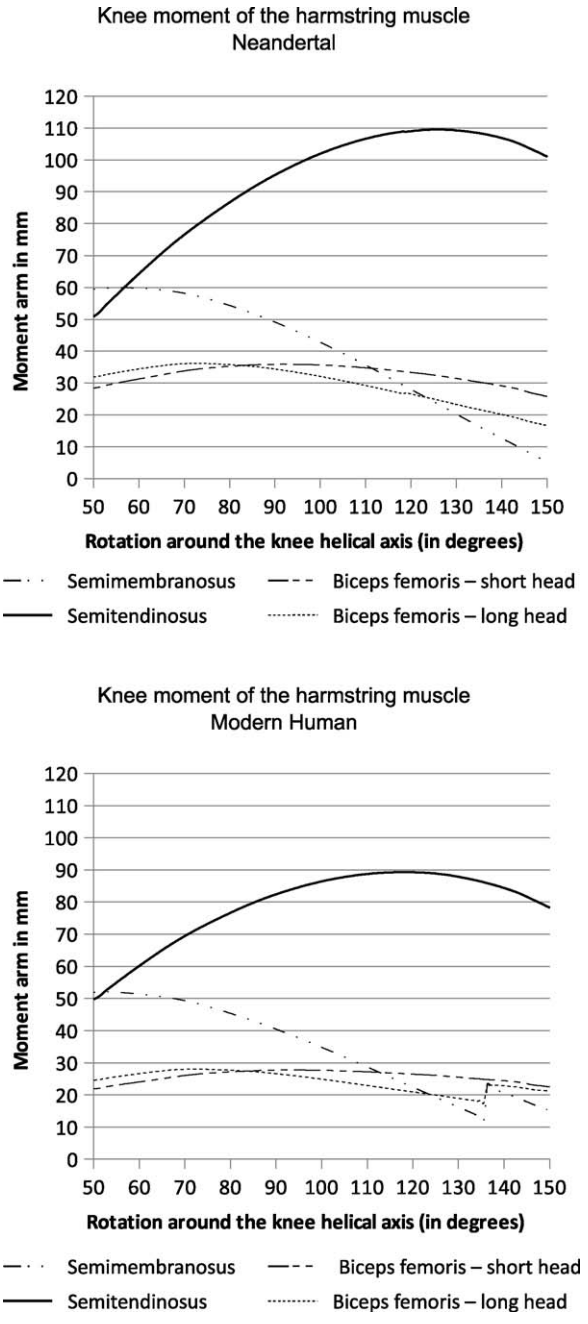

Fig. 5. Comparative motion graphs and knee moment arm graphs of hamstring muscles of Neandertals (left) and humans (right). Moment arms are given in mm.

Fig. 5. Comparaison des courbes de mouvements (en degrés) et des moments musculaires (en mm) au niveau de l'articulation du genou des muscles ischiojambiers entre Néandertalien (à gauche) et Homme moderne (à droite).

Kepple et al. (1998) stated that there is a wide range of pelvic differences within a single species, not only between males and females but also between females of different geographic origin. Pelvis RMS errors were therefore

divided into separate models (male model (RMS errors of 8.6 mm), and different female geographic origins models (7.0 mm) and (7.3 mm)) as RMS errors were too high to report between all specimens (Kepple et al., 1998). Spatial data registration from the Kebara 2 pelvis to the Neandertal 1 pelvis gave an RMS error of 10.8 mm from one iliac bone. There are several factors, which may account for this slightly higher error. The Kebara 2 pelvis was found in Israel and the Neandertal 1 pelvis was found in Germany (Schmitz et al., 2002). There is a time difference of approximately 10,000–15,000 years between the two pelves, which could account for changes (Bar-Yosef et al., 1992; Schmitz et al., 2002). The Kebara 2 pelvis has been widely documented as being a male (Bar-Yosef et al., 1992) although no information is available for the sex of the Neandertal 1 skeleton, which could potentially be male or female. While every effort is made to minimize errors in the data processing pipeline there may be errors due to differences in palpation (Van Sint Jan and Della Croce, 2005). Another source of error could be linked to the specimen preservation: for example, when bone areas are missing. However, the method presented here focuses on anatomical landmarks that are the same in all specimens, therefore reducing the probability of error due to missing areas.

4.2. Use of the virtual modeling for biomechanical analysis

The final aim of this study was to apply a particular motion pattern, collected from a modern day human, to the Neandertal skeleton to determine if the final results support the initial hypothesis that bone morphology and joint surfaces of Neandertals demonstrate similar motion patterns to anatomically modern humans. Standard registration techniques of bone morphology to motion data analysis often lead to unsatisfactory motion simulation because of discrepancies during the location of anatomical landmarks in the datasets. The adoption of a method that allows integration of six DOFs in the joint (Sholukha et al., 2006) enables a more realistic analysis of gliding of joint surfaces during motion and detection, e.g., unrealistic bone collisions or joint dislocations due to incompatible joint surfaces within a given motion pattern. Observation of the reconstructed simulation demonstrated that the joint surfaces of the Neandertal model show a good compatibility with general motion patterns performed by a modern human. For example, the Neandertal joint surface remains congruent during the full range of motion. This is obviously an assumption since real motion measurements cannot be collected on the extinct Neandertal individuals. However, the above joint congruence is an important step towards the obtained fusion results for further biomechanical muscle study as performed in this paper.

The robust skeletal morphology of the Neandertal has been interpreted as an adaptation for cold (Weaver, 2003), for frequently elevated levels of biomechanical stress (Trinkaus, 1983) or consistent with higher mechanical loads (Ruff et al., 1993; Trinkaus and Ruff, 1989; Trinkaus et al., 1994). Stock (2006) in a recent study on hunter-gatherer groups found that robusticity of segments correlate negatively with climate and positively with patterns of terrestrial and marine mobility. This is also a conclusion drawn by Trinkaus (1983) who stated that the robustness demonstrated across all Neandertal specimens meant that is was most likely an adaptation to behaviour.

Hamstring moment arms found in this paper for modern humans are similar to previously reported results (e.g. Bonnefoy et al., 2007, who utilize several different musculoskeletal models) indicating the method is sound. In Neandertals, robustness seems to be proportional to mechanical advantage, at least for the hamstring muscles, and mechanical advantage was found to be much greater in Neandertals than in modern humans. This result is consistent with earlier findings that if we assume a modern human-like locomotion in Neandertals then they may have had a higher mechanical advantage, greater bending moments and larger moment arms as opposed to modern humans (e.g. Ruff, 1995, 2009; Trinkaus, 1983; Trinkaus and Ruff, 1989).

This preliminary study was limited to the analysis of the hamstring muscles. Further studies will concentrate on developing a full muscular skeletal analysis of the lower limb of the Neandertal. In order to be more representative we also aim to include more than one Neandertal specimen, as we did in this study. The method presented and software tools allow for further analytical studies to be performed to enable the study of the relationships between hominid morphology and mechanical efficiency of the musculoskeletal system. This software will enable further comparative analysis between all hominid species.

Acknowledgements

We thank Mr. Hakim Bajou (LABO, ULB) for his technical assistance and the team at the Radiology Department of the ULB Erasme Hospital for scanning the fossil material. Jean-Louis Lufimpadio for his technical help in segmenting the CT data. CT scans from the Spy fossils are available on request from the Nespos database (http://www.nespos.org/). lhpFusionBox was orginally developed as part of the LHDL project using the MAF application framework developed by the BioComputing Competence Center, Bologna, Italy. http://www.openmaf.org.

References

Andersen, C.R., 1989. Neandertal pelves and gestation length: Hypotheses and holism in Paleoanthropology. Am. Anthropol. 91, 327–340.

Bar-Yosef, O., Vandermeersch, B., Arensburg, B., Belfer-Cohen, A., Goldberg, P., Laville, H., Meignen, L., Rak, Y., Speth, J.D., Tchernov, E., Tillier, A.M., Weiner, S., 1992. The excavations in Kebara Cave Mount Carmel. Curr. Anthropol. 33, 497–550.

Benazzi, S., Orlandi, M., Grupponi, G., 2009. Technical note: Virtual reconstruction of a fragmentary clavicle. Am. J. Phys. Anthropol. 138, 507–514.

Berge, C., Goularas, B., 2010. A new reconstruction of Sts 14 pelvis (*Australopithecus africanus*) from computed tomography and three-dimensional modeling techniques. J. Hum. Evol. 58, 262–272.

Bonnefoy, A., Doriot, N., Senk, M., Dohin, B., Pradon, D., Chèze, L., 2007. A non-invasive protocol to determine the personalized moment arms of knee and ankle muscles. J. Biomech. 40, 1776–1785.

Brand, P.W., Hollister, A., 1992. Clinical Mechanics of the Hand. Mosby Year Book, St. Louis, 369 p.

Challis, J.H., 1995. A procedure for determining rigid body transformation parameters. J. Biomech. 26, 733–737.

Chapman, T., Van Sint Jan, S., Moiseev, F., Louryan, S., Rooze, M., in press. From Modern Humans to Spy Ancestors? Comparison of the locomotion of anatomically modern humans and Neandertals (Spy II): A feasibility study. In: Semal P., Rougier H., Jungels C., Hauzeur A. (Eds.), Spy Cave. State of 120 years of pluridisciplinary research on the Betche-aux-Rotches from Spy (Jemeppe-sur-Sambre, Province of Namur, Belgium). Royal Belgian Institute of Natural Sciences and NESPOS Society, Brussels.

Delp, S.L., Loan, J.P., Hoy, M.G., Zajac, F.E., Topp, E.L., Rosen, J.M., 1990. An interactive graphics-based model of the lower extremity to study orthopaedic surgical procedures. IEEE. Trans. Biomed. Eng. 37, 757–767.

Gruss, L.T., 2007. Limb length and locomotor biomechanics in the genus Homo: An experimental study. Am. J. Phys.Anthropol. 134, 106–116.

Gunz, P., Mitteroecker, P., Bookstein, F.L., Weber, G.W., 2004. Computer aided reconstruction of incomplete human crania using statistical and geometrical estimation methods. Enter the past: Computer applications and quantitative methods in archaeology. BAR. Int. Ser. 1227, 92–94.

Gunz, P., Mitteroecker, P., Neubauer, S., Weber, G.W., Bookstein, F.L., 2009. Principles for the virtual reconstruction of hominin crania. J. Hum. Evol. 57, 48–62.

Hrdlička, A., 1930. The skeletal remains of early man. Smiths. Misc. Coll. 83, 1–379.

Horn, B.K.P., 1987. Closed-form solution of absolute orientation using unit quaternions. J. Opt. Soc. Am. 4, 629–642.

Kalvin, A.D., Dean, D., Hublin, J.J., 1995. Reconstruction of human fossils. IEEE. Comput. Graph. Applicat. 15, 12–15.

Kepple, T.M., Sommer III, H.J., Siegel, K.L., Stanhope, S.J., 1998. A three-dimensional musculoskeletal database for the lower extremities. J. Biomech. 31, 77–80, http://pdb.cc.nih.gov/resources/files/terry/terry.htm.

Kramer, P.A., Eck, G.G., 2000. Locomotor energies and leg length in hominid bipedality. J. Hum. Evol. 38, 651–666.

Leakey, M.G., Leakey, R.E., Richtsmeier, J.T., Simons, E.L., Walker, A.C., 1991. Morphological similarities in *Aegyptopithecus* and *Afropithecus*. Folia Primatol. 56, 65–85.

Lieber, R.L., 2002. Skeletal Muscle Structure, Function and Plasticity: The Physiological Basis of Rehabilitation. Lippincott Williams and Wilkins, Baltimore, 448 p.

Miller, J.A., Gross, M.M., 1998. Locomotor advantages of Neandertal skeletal morphology at the knee and ankle. J. Biomech. 31, 355–361.

Neubauer, S., Gunz, P., Mitteroecker, P., Weber, G.W., 2004. Three-dimensional digital imaging of the partial *Australopithecus africanus* endocranium MLD 37/38. Can. Assoc. Radiol. J. 55, 271–278.

Nicolas, G., Multon, F., Berillon, G., Marchal, F., 2007. From bone to plausible bipedal locomotion using inverse kinematics. J. Biomech. 40, 1048–1057.

Nicolas, G., Multon, F., Berillon, G., 2009. From bone to plausible bipedal locomotion. Part II: Complete motion synthesis for bipedal primates. J. Biomech. 42, 1127–1133.

Polk, J.D., 2004. Influence of limb proportions and body size on locomotor kinematics in terrestrial primates and fossil hominins. J. Hum. Evol. 47, 237–252.

Ponce de León, M.S., Zollikofer, C.P.E., 1999. New evidence from Le Moustier 1: Computer-assisted reconstruction and morphometry of the skull. Anat. Rec. 254, 474–489.

Ponce de León, M.S., Golovanova, L., Doronichev, V., Romanova, G., Akazawa, T., Kondo, O., et al., 2008. Neanderthal brain size at birth provides insights into the evolution of human life history. Proc. Natl. Acad. Sci. 105, 13764–13768.

Rak, Y., 1991. The pelvis. In: Bar-Yosef, O., Vandermeersch, B. (Eds.), Le Squelette Moustérien de Kébara 2, Mt. Carmel, Israel. CNRS, Paris, pp. 147–156.

Rak, Y., Arensburg, B., 1987. Kebara 2 Neanderthal iliac: First look at a complete inlet. Am. J. Phys. Anthropol. 73, 227–231.

Ruff, C.B., Trinkaus, E., Walker, A., Larsen, C.S., 1993. Postcranial robusticity in Homo. I: temporal trends and mechanical interpretation. Am. J. Phys.Anthropol 91, 21–53.

Ruff, C.B., 1995. Biomechanics of the hip and birth in early *Homo*. Am. J. Phys. Anthropol. 98, 527–574.

Ruff, C.B., 2009. Relative limb strength and locomotion in *Homo habilis*. Am. J. Phys. Anthropol. 138, 90–100.

Sawyer, G.J., Maley, B., 2005. Neanderthal reconstructed. Anat. Rec. (Part B: New Anat.) 283B, 23–31.

Schmitz, R.W., Serre, D., Bonani, G., Feine, S., Hillgruber, F., Krainitzki, H., Pääbo, S., Smith, F.H., 2002. The Neandertal type site revisited: Interdisciplinary investigations of skeletal remains from the Neander Valley. Germany. Proc. Natl. Acad. Sci. 99, 13342–13347.

Sellers, W.I., Dennis, L.A., Wang, W.-J., Crompton, R.H., 2004. Evaluating alternative gait strategies using evolutionary robotics. J. Anat. 204, 343–351.

Semal, P., Rougier, H., Crevecoeur, I., Jungels, C., Flas, D., Hauzeur, A., Maureille, B., Germonpré, M., Bocherens, H., Pirson, S., Cammaert, L., De Clerck, N., Hambucken, A., Higham, T., Toussaint, M., van der Plicht, J., 2009. New data on the late Neandertals: Direct dating of the Belgian Spy Fossils. Am. J. Phys. Anthropol. 138, 421.

Sholukha, V., Leardini, A., Salvia, P., Rooze, M., Van Sint Jan, S., 2006. Double-step registration of in vivo stereophotogrammetry with both in vitro electrogoniometry and CT medical imaging. J. Biomech. 39, 2087–2095.

Steudel-Numbers, K.L., Tilkens, M.J., 2004. The effect of lower limb length on the energetic cost of locomotion: Implications for fossil hominins. J. Hum. Evol. 47, 95–109.

Stock, J.T., 2006. Hunter-gatherer postcranial robusticity relative to patterns of mobility, climatic adaptation, and selection for tissue economy. Am. J. Phys. Anthropol. 131, 194–204.

Trinkaus, E., 1981. Neanderthal limb proportions and cold adaptation. In: Stringer, C.B. (Ed.), Aspects of Human Evolution. Taylor and Francis, London, pp. 21–53.

Trinkaus, E., 1983. The Shanidar Neanderthals. Academic Press, New York, 502 p.

Trinkaus, E., 1985. Pathology and the Posture of the La Chapelle-aux-Saints Neandertal. Am. J. Phys. Anthropol. 67, 19–41.

Trinkaus, E., Ruff, C.B., 1989. Diaphyseal cross-sectional morphology and biomechanics of the Fond-de-Forêt 1 femur and the Spy 2 femur and tibia. Bull. Soc. R. Belge. Anthropol. Prehist. 100, 33–42.

Trinkaus, E., Churchill, S.E., Ruff, C.B., 1994. Postcranial robusticity in Homo. II: humeral bilateral asymmetry and bone plasticity. Am. J. Phys.Anthropol. 93, 1–34.

Trinkaus, E., Ruff, C.B., Churchill, S.E., Vandermeersch, B., 1998. Locomotion and body proportions of the Saint-Césaire 1 Châtelperronian Neandertal. Proc. Natl. Acad. Sci. U S A 95, 5836–5840.

Van Sint Jan, S., 2007. Color Atlas of Skeletal Landmark Definitions; Guidelines for Reproducible Manual and Virtual Palpations. Churchill Livingstone Elsevier, Edinburgh, 208 p.

Van Sint Jan, S., Della Croce, U., 2005. Accurate palpation of skeletal landmark locations: Why standardized definitions are necessary. A proposal. Clin. Biomech. 20, 659–660.

Van Sint Jan, S., Demondion, X., Louryan, S., Clapworthy, G., Rooze, M., Cotton, A., Viceconti, M., 2006. Multimodal visualisation interface for data management, self-learning and data presentation. Surg. Radiol. Anat. 28, 518–524.

Van Sint Jan, S., Salvia, P., Hilal, I., Sholukha, V., Rooze, M., Clapworthy, G., 2002. Registration of 6-DOFs electrogoniometry and CT medical imaging for 3D joint modeling. J. Biomech. 35, 1475–1484.

Viceconti, M., Taddei, F., Montanari, L., Testi, D., Leamidi, A., Clapworthy, G., Van Sint Jan, S., 2007a. Multimod Data Manager: A tool for data fusion. Comput. Methods Programs Biomed. 87, 148–159.

Viceconti, M., Zannoni, C., Testi, D., Petrone, M., Perticoni, S., Quadrani, P., Taddei, F., Imboden, S., Clapworthy, G., 2007b. The multimod application framework: A rapid application development tool for computer aided medicine. Comput. Methods Programs Biomed. 85, 138–151.

Weaver, T.D., 2003. The shape of the Neandertal femur is primarily the consequence of a hyperpolar body form. PNAS 100, 6926–6929.

Weaver, T.D., Hublin, J.J., 2009. Neandertal birth canal shape and the evolution of human childbirth. PNAS 106, 8151–8156.

Wu, G., Siegler, S., Allard, P., Kirtley, C., Leardini, A., Rosenbaum, D., Whittle, M., D'Lima, D., Cristofolini, L., Witte, H., Schmid, O., and Stokes, I., 2002. ISB recommendation on definitions of joint coordinate systems of various joints for the reporting of human joint motion-Part I: ankle, hip, spine. J. Biomech. 35, 543–548.